

Integrated electro-optic modulator on lead zirconate titanate-silicon nitride heterogeneous platform

WENFENG ZHOU,¹ YONG ZHANG,^{1, 2,*} YONGHENG JIANG,³ PU ZHANG,³ JIAN SHEN,¹ XUN ZHANG,¹ YUQI CHEN,¹ MIN SUN,¹ FENG QIU,⁴ HUIFU XIAO,^{3,*} YONGHUI TIAN,³ AND YIKAI SU¹

¹*State Key Lab of Advanced Optical Communication Systems and Networks, Department of Electronic Engineering, Shanghai Jiao Tong University, Shanghai 200240, China*

²*State Key Laboratory of Precision Spectroscopy, East China Normal University, Shanghai 200241, China*

³*School of Physical Science and Technology, Lanzhou University, Lanzhou, Gansu 730000, China*

⁴*Hangzhou Institute for Advanced Study, University of Chinese Academy of Sciences, Zhejiang, Hangzhou 310024, China*

*Corresponding author:

yongzhang@sjtu.edu.cn

xiaohf@lzu.edu.cn

Received XX Month XXXX; revised XX Month, XXXX; accepted XX Month XXXX; posted XX Month XXXX (Doc. ID XXXXX); published XX Month XXXX

Integrated electro-optic (EO) modulators are the core components of optoelectronic information technology, and lithium niobate is currently the most widely used crystalline thin film material, however, finite EO coefficients limit the modulation efficiency of the modulators. In this letter, we present an integrated EO modulator using microring resonator on the lead zirconate titanate (PZT) and silicon nitride (SiN) heterogeneous platform. The microwave attenuation is reduced by using low dielectric constant SiN as the electrode substrate, achieving an EO bandwidth of 33 GHz. Thanks to the high quality of the PZT film deposition and the substantial EO overlap of our structure, ultra-high modulation efficiency with the half-wave voltage-length product of 0.7 V·cm is achieved. In addition, as a remarkable result, an 80-Gbps on-off keying signal is generated using the modulator.

Integrated electro-optic (EO) modulators can modulate electrical signals to light-waves in high-speed way, which are widely used in optical communications networks [1], photo computing [2], quantum photonics [3] and programmable integrated circuits [4]. There are various physical effects to realize EO modulators, such as free-carrier dispersion effect [5], electro-absorption effect [6], and Pockels effect [7]. For the first two effects, one of the popular material platforms is silicon-on-insulator (SOI). It exhibits the advantages of CMOS compatibility and compactness [8,9], however, free carrier dispersion is absorbing and nonlinear, which not only reduces the modulation amplitude but also leads to distortion in advanced modulation formats. Silicon poses a significant challenge for the future realization of high baud rate transmissions as well as power consumption due to its lack of inherent second-order nonlinearity [10]. Fortunately, the Pockels effect enables ultrafast and pure refractive index modulation over a very wide spectral range without introducing additional losses [11]. Therefore, the heterogeneous integration of various new EO functional materials

on silicon substrates has attracted great interest, including lithium niobate (LiNbO_3 , LN) [12], lithium tantalite (LiTaO_3 , LT) [13], aluminum nitride (AlN) [14], barium titanate (BaTiO_3 , BTO) [15] and silicon carbide (SiC). LN shows good results in high baud rate multilevel signals due to its EO effect and low-loss optical transmission. However, the EO coefficient of LN is limited to 30 pm/V, which results in a half-wave voltage-length product ($V_{\pi}L$) controlled within 2~4 V·cm [16].

Lead zirconate titanate ($\text{PbZr}_x\text{Ti}_{1-x}\text{O}_3$, PZT) has a large bandgap (4.1 eV) [17], low loss, and an EO coefficient four times higher than LN [18]. These advantages make it a promising candidate for EO modulators. In early works, the PZT microring EO modulator has been fabricated by depositing PZT film on SiN waveguides using the chemical solution deposition (CSD) method [19]. However, the imperfect SiN waveguide surface planarization process degrades the quality of the PZT film, limiting $V_{\pi}L$ to 3.3 V·cm. By removing the SiN waveguide underneath the PZT film and depositing the PZT film on a flat silicon oxide (SiO_2) substrate, the quality of the PZT film is improved, achieving a modulation efficiency of 1.17 V·cm [20]. Yet, the high dielectric constant of PZT contributes to large microwave attenuation, limiting the bandwidth of the modulator to 24 GHz.

In this letter, we demonstrate a high-speed and high-efficiency microring modulator on a SiN loaded PZT platform. The high-quality PZT thin film is fabricated by the CSD method on a flat SiO_2/Si substrate. Non-etching of PZT film achieves a high EO coefficient of up to 84 pm/V. Benefiting from a large EO overlap factor of 0.6, the microring modulator achieves a $V_{\pi}L$ as low as 0.7 V·cm. Microwave attenuation is effectively reduced by placing the electrodes on the SiN film with a low dielectric constant. The modulator achieves a modulation bandwidth of 33 GHz and successfully generates an 80-Gbps on-off keying (OOK) signal.

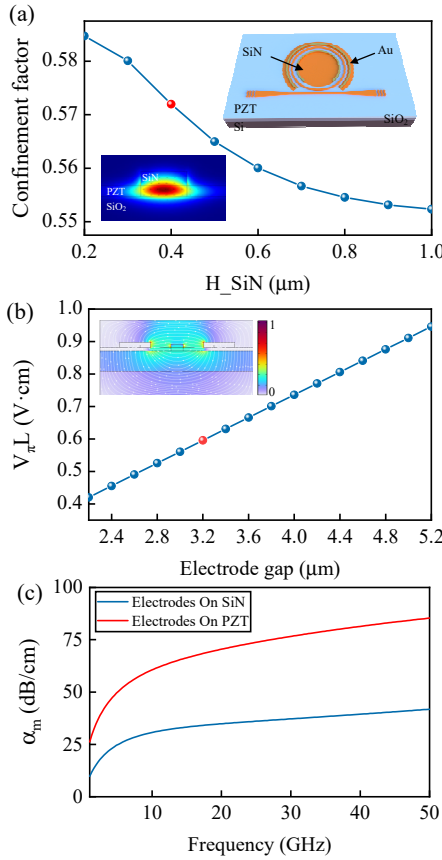


Fig. 1. (a) Relation between the energy confinement factor in the PZT layer and the thickness of the SiN waveguide. Insets: Electric field of the fundamental TE mode and schematic diagram of PZT-SiN heterogeneous integrated microring EO modulator. (b) Modeling the relationship between the $V_{\pi}L$ and the electrodes gap. Inset: Electric field distribution (applied electric field 1V). The red sphere shows the parameters used in this work. (c) Microwave attenuation of electrodes placed on SiN film (blue curve) and PZT film (red curve), respectively.

The schematic diagram of the proposed PZT-SiN heterogeneous integrated microring EO modulator is shown in the inset of Fig. 1(a). The SiN waveguide is placed on a 300 nm PZT layer to guide the light wave. The higher refractive index of PZT (~ 2.4) compared to SiN (~ 2) ensures that the light field propagates within the PZT layer. Fig. 1(a) shows the optical field energy confinement factor in the PZT layer as a function of SiN thickness calculated using the finite element method. Increasing the SiN thickness gradually reduces the percentage of the optical field confined within the PZT waveguide. Setting the SiN waveguide thickness to 400 nm and width to 1.2 μm achieves an optical field confinement factor in the PZT layer exceeding 57%, enabling effective utilization of the strong EO coefficients in PZT. The inset in Fig. 1(a) illustrates the electric field in the fundamental TE mode, with a calculated effective refractive index of the hybrid waveguide being 2.03 at 1550 nm. The high modulation efficiency relies on a substantial EO overlap. The theoretical EO overlap and $V_{\pi}L$ can be expressed by the following equation [19]:

$$\Gamma = \frac{g}{V} \frac{\epsilon_0 c n_{PZT} \iint_{PZT} E_x^e |E_x^o|^2 dx dy}{\iint_{all} \text{Re}(E^o \times H^{o*}) \cdot \hat{e}_z dx dy}, \quad (1)$$

$$V_{\pi}L = \frac{\lambda_0 \cdot g}{n_{PZT}^3 \Gamma r_{eff}}, \quad (2)$$

where g is the gap between the electrodes, V is the applied voltage, ϵ_0 is the vacuum permittivity, c is the speed of light in vacuum, n_{PZT} is the refractive index of PZT, E_x^o and E_x^e are the in-plane (x-) transversal components of the optical field and the electric field, respectively, λ_0 is the resonance wavelength. Fig. 1(b) shows that as the electrodes gap is reduced, the $V_{\pi}L$ decreases correspondingly. In order to achieve the optimal balance between modulation efficiency and electrodes metal absorption of the optical field, the gap between the electrodes is 3.2 μm, with a theoretically $V_{\pi}L$ of 0.6 V·cm, which benefits from an EO overlap of 0.6.

Microwave attenuation limits EO performance at high frequencies, and high dielectric constants often lead to increased microwave attenuation [21]. We use finite element methods to simulate the microwave attenuation of electrodes on PZT and SiN thin film. Fig. 1(c) illustrates that electrodes placed on SiN film exhibit significantly lower microwave attenuation compared to placing on PZT film, primarily due to the relative permittivity of PZT film being two orders of magnitude higher than SiN film.

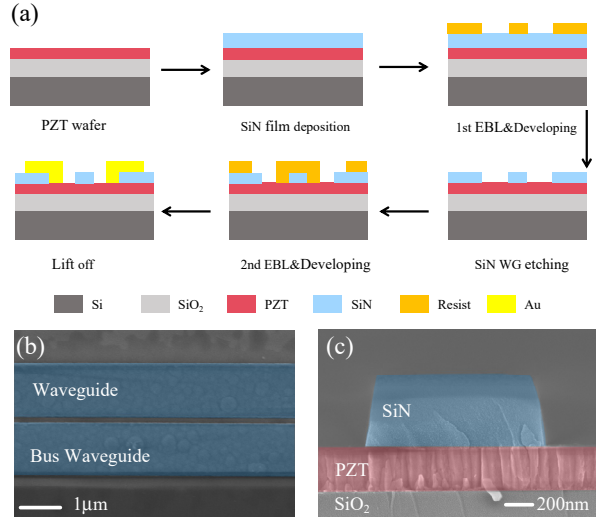


Fig. 2. (a) Schematic of the fabrication process of the PZT-SiN integrated microring EO modulator. (b) False-color SEM image of the bus waveguide and ring waveguide. (c) False-color SEM image of the waveguide cross section.

In the experiment, a 300-nm-thick PZT thin film is deposited on a substrate consisting of a 2-μm-thick SiO₂ layer and a 525-μm-thick Si layer using the CSD method. A 400nm SiN film is deposited using plasma enhanced chemical vapor deposition (PECVD, Oxford). Subsequently, the patterns including gratings and microrings are defined on the resist (AR-P6200.09) using e-beam lithography (EBL, Vistec EBPG 5200*). Inductively Coupled Plasma (ICP) dry etching transfers the patterns to the SiN layer. In a subsequent step of EBL and electron beam evaporation, 300 nm of gold is deposited on a 10 nm thick Ti adhesive layer, forming electrodes and pads through the lift-off process. Fig. 2 illustrates a detailed flow diagram and false-color scanning electron microscope (SEM) images of the fabricated device.

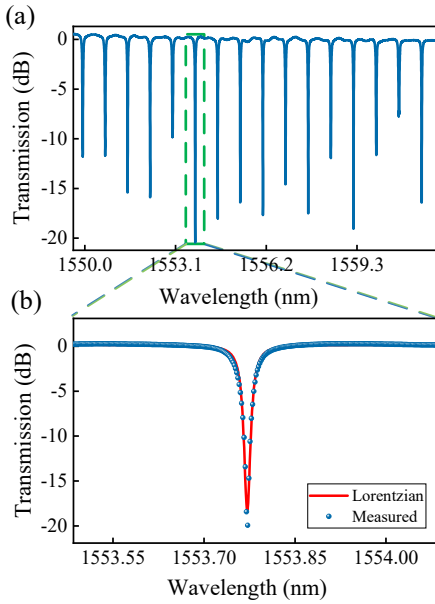


Fig. 3. (a) Measured normalized transmission spectrum of the PZT-SiN microring. (b) Lorentz fitting (red curve) of the resonance dip at 1553.7nm.

The transmission spectrum of the fabricated PZT-SiN microring is characterized in the C-band using a tunable laser scanning system (EXFO T100S-HP-CLU-M-CTP10-00). On-chip grating couplers are used to couple the light into/out of the hybrid SiN-PZT optical waveguide. The measured coupling loss is 6 dB/face. To minimize the effect of bending losses, a microring radius of 200 μm is used. Fig. 3(a) shows the transmission spectrum normalized to the grating couplers for wavelengths around 1550 nm. Lorentz curve fitting reveals a measured Q of 4.4×10^4 at 1553 nm, an intrinsic Q of 8.2×10^4 , an extinction ratio of 20.79 dB, and a free spectral range (FSR) of 0.773 nm in Fig. 3(b). Equation 3 can be used to calculate the propagation loss of the PZT-SiN hybrid waveguide [22].

$$\alpha = \frac{2 \cdot \pi \cdot n_g}{Q_i \cdot \lambda_0} = \frac{\lambda_0}{Q_i \cdot R \cdot FSR}, \quad (3)$$

where α is the propagation loss per unit length, n_g , Q_i , and R represent the group refractive index, intrinsic Q , and microring radius, respectively. The propagation loss of the hybrid waveguide is calculated to be 1.2 cm^{-1} . The loss can be further mitigated by optimizing the film deposition process and reducing surface and sidewall roughness to minimize light scattering losses.

The PZT film lacks an EO effect due to its in-plane dipole orientation relative to the surface normal, requiring electric field polarization to induce the dipole characteristics of the ferroelectric state [23]. We apply a voltage of 48 V ($\approx 150 \text{ kV cm}^{-1}$) to the electrodes for 1 hour at elevated temperatures to obtain optimal EO response. Fig. 4(a) illustrates the linear shift of the microring resonance wavelength with applied voltage. The resonance wavelength is blue-shifted by 1.1 nm as the voltage varies from 0 V to 20 V. The fitting linear tuning efficiency is 58 pm/V in Fig. 4(b). Moreover, the measured modulation efficiency can be represented by $V_{\pi L}$ according to the equation: $V_{\pi L} = |L \cdot FSR \cdot \Delta V / (2\Delta\lambda)| \approx 0.7 \text{ V}\cdot\text{cm}$, which is close to the simulation results. The remarkable

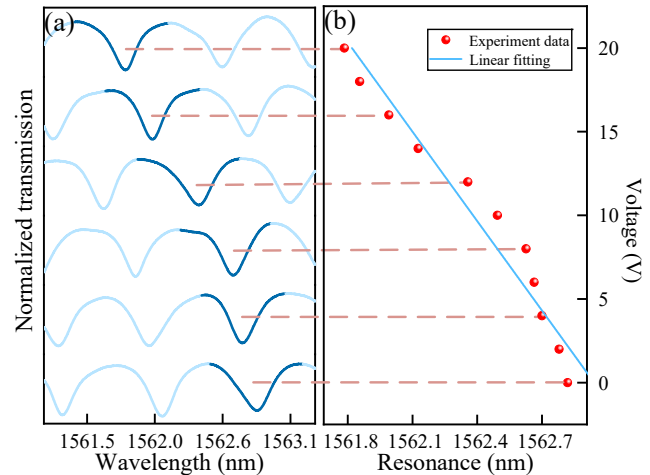


Fig. 4. (a) Normalized transmission spectra of PZT-SiN microring at different voltages. (b) Resonance wavelength shift with versus voltage and tuning efficiency of linear fitting.

modulation efficiency can be attributed to two crucial factors: the profoundly high EO overlap and the notably high EO coefficient of the PZT thin films. Specifically, the EO coefficient is calculated to be 84 pm/V. The EO coefficient improvement is attributed to the high quality deposited on a uniform SiO_2/Si substrate while avoiding the effects of direct etching of PZT on the EO performance.

To investigate the EO response of the modulator, we characterize the EO S_{21} responses of the microring modulators using a 67 GHz lightwave component analyzer (LCA, Keysight N5227B). Fig. 5(a) illustrates the EO S_{21} response of the fabricated modulator, with a measured 3-dB bandwidth of 33 GHz.

Finally, the modulator is tested using a high-speed driving signal. The OOK signal generated by the arbitrary waveform generator (AWG, Keysight M8195A) and amplified by the RF amplifier (SHF 807C) with a peak-to-peak voltage of ~ 2 V is applied to the electrodes via the GS probe. The wavelength is selected at the position where the optical power decreases by 3 dB. The modulated light is then detected by a high-speed photodetector (PD, Finisar XPDV3120) and analyzed using a digital storage oscilloscope (DSO, Keysight N1092). 60-Gbps, 70-Gbps, and 80-Gbps OOK signals are successfully generated, where the signal-to-noise ratios (SNRs) of the OOK signals reach 5.4dB, 3.1dB, and 2.47dB, respectively, as shown in Fig. 5(b).

Table 1 compares the performance of the State-of-the-Art PZT and lithium niobate on insulator (LNOI) microring EO modulator. In comparison to the method of growing PZT film on a SiN waveguide, the deposition of PZT film on uniform SiO_2/Si substrate by CSD method followed by the formation of a waveguide with SiN film, avoids the etching of PZT. This approach results in improved PZT film quality and a nearly five times increase in modulation efficiency. In contrast to the direct etching of the PZT film, a low-dielectric-constant SiN film is introduced to form waveguides and reduce microwave losses, resulting in higher modulation bandwidth and enabling the generation of higher-speed OOK signals. The

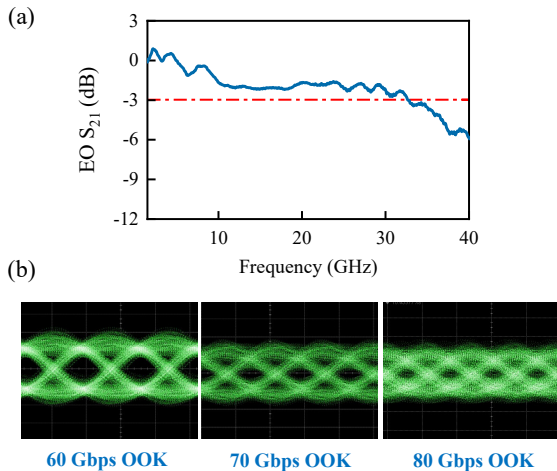


Fig. 5. (a) Measured EO S_{21} responses. (b) Measured eye diagrams for the OOK signal with the data rate of 60 Gbps, 70 Gbps, and 80 Gbps respectively.

modulator exhibits higher modulation efficiency compared to LNOI microring modulators.

Table 1. Performance of the State-of-the-Art PZT and LNOI microring EO modulators.

Platform	Modulation efficiency	Bandwidth	Date Rate
PZT-SiN [19]	3.30 V·cm	33 GHz	40 Gbps OOK
PZT [20]	1.17 V·cm	24 GHz*	56 Gbps OOK
LNOI [24]	9.10 V·cm	5 GHz	9 Gbps OOK
LNOI [25]	n/a	30 GHz	40 Gbps OOK
This work	0.70 V·cm	33 GHz	80 Gbps OOK

* Calculated bandwidth, n/a not available.

In conclusion, we demonstrate a high-speed and high-efficiency PZT-SiN heterogeneous integrated microring modulator. PZT film is deposited on flat surfaces and avoids etching, thus providing high-quality PZT film with an EO coefficient of 84 pm/V and a modulation efficiency of 0.7 V·cm. By using a low-dielectric-constant SiN layer, the device bandwidth reaches 33 GHz, and in particular, an 80-Gbps OOK signal is successfully generated using the modulator. The proposed PZT-SiN platform will provide new insights for the development of high-efficiency, low-cost, and high-speed EO modulators and lay the foundation for low-power consumption programmable photonics.

Funding

National Key R&D Program of China under Grant No. 2020YFB2206101; National Natural Science Foundation of China (NSFC) (62335014/62035016/62341508).

Acknowledgments. We thank the Center for Advanced Electronic Materials and Devices (AEMD) of Shanghai Jiao Tong University (SJTU) for the device fabrication.

Disclosures. The authors declare no conflicts of interest.

Data availability. Data underlying the results presented in this paper are not publicly available at this time but may be obtained from the authors upon reasonable request.

References

- D. A. B. Miller, *J. Lightwave Technol* **35**, 346 (2017).
- C. Sun, M. T. Wade, Y. Lee, J. S. Orcutt, L. Alloatti, M. S. Georgas, A. S. Waterman, J. M. Shainline, R. R. Avizienis, S. Lin, B. R. Moss, R. Kumar, F. Pavanello, A. H. Atabaki, H. M. Cook, A. J. Ou, J. C. Leu, Y. H. Chen, K. Asanovic, R. J. Ram, M. A. Popovic, and V. M. Stojanovic, *Nature* **528**, 534 (2015).
- X. D. Zheng, P. Y. Zhang, R. Y. Ge, L. L. Lu, G. L. He, Q. Chen, F. C. Qu, L. B. Zhang, X. L. Cai, Y. Q. Lu, S. N. Zhu, P. H. Wu, and X. S. Ma, *Adv. Photonics* **3**, 10 (2021).
- Y. H. Zhao, X. Wang, D. S. Gao, J. J. Dong, and X. L. Zhang, *Front. Optoelectron* **12**, 148 (2019).
- Q. F. Xu, B. Schmidt, S. Pradhan, and M. Lipson, *Nature* **435**, 325 (2005).
- J. Liu, M. Beals, A. Pomerene, S. Bernardis, R. Sun, J. Cheng, L. C. Kimerling, and J. Michel, *Nat. Photonics* **2**, 433 (2008).
- M. B. He, M. Y. Xu, Y. X. Ren, J. Jian, Z. L. Ruan, Y. S. Xu, S. Q. Gao, S. H. Sun, X. Q. Wen, L. D. Zhou, L. Liu, C. J. Guo, H. Chen, S. Y. Yu, L. Liu, and X. L. Cai, *Nat. Photonics* **13**, 359 (2019).
- L. P. Gu, B. B. Wang, Q. C. Yuan, L. Fang, Q. Zhao, X. T. Gan, and J. L. Zhao, *APL Photonics* **6**, 6 (2021).
- Y. He, Y. Zhang, Q. M. Zhu, S. H. An, R. Y. Cao, X. H. Guo, C. Y. Qiu, and Y. K. Su, *J. Lightwave Technol* **36**, 5746 (2018).
- G. T. Reed, G. Mashanovich, F. Y. Gardes, and D. J. Thomson, *Nat. Photonics* **4**, 518 (2010).
- M. Zhang, C. Wang, P. Kharel, D. Zhu, and M. Loncar, *Optica* **8**, 652 (2021).
- Y. Zhang, J. Shen, J. C. Li, H. W. Wang, C. L. Feng, L. Zhang, L. Sun, J. Xu, M. Liu, Y. Wang, Y. H. Tian, J. W. Dong, and Y. K. Su, *Light-Sci. Appl* **12**, 10 (2023).
- J. Shen, Y. Zhang, C. L. Feng, Z. H. Xu, L. Zhang, and Y. K. Su, *Opt. Lett* **48**, 6176 (2023).
- Z. H. Xu, Y. Zhang, J. Shen, Y. H. Dong, L. Y. Wu, J. Xu, and Y. K. Su, *Opt. Lett* **47**, 4925 (2022).
- S. Abel, F. Eltes, J. E. Ortmann, A. Messner, P. Castera, T. Wagner, D. Urbonas, A. Rosa, A. M. Gutierrez, D. Tulli, P. Ma, B. Baeuerle, A. Josten, W. Heni, D. Caimi, L. Czornomaz, A. A. Demkov, J. Leuthold, P. Sanchis, and J. Fompeyrine, *Nat. Mater* **18**, 42 (2019).
- G. Y. Chen, Y. Gao, H. L. Lin, and A. J. Danner, *Adv. Photon. Res* **4**, 15 (2023).
- X. H. Du, J. H. Zheng, U. Belegundu, and K. Uchino, *Appl Phys Lett* **72**, 2421 (1998).
- D. S. Ban, G. L. Liu, H. Y. Yu, X. Y. Sun, N. P. Deng, and F. Qiu, *Opt. Mater. Express* **11**, 1733 (2021).
- K. Alexander, J. P. George, J. Verbist, K. Neyts, B. Kuyken, D. Van Thourhout, and J. Beeckman, *Nat. Commun* **9**, 6 (2018).
- G. L. Liu, H. Y. Yu, D. S. Ban, B. Li, G. Q. Wei, C. Yang, J. G. Wang, Y. I. Sohn, Y. Han, and F. Qiu, *APL Photonics* **9**, 6 (2024).
- P. Kharel, C. Reimer, K. Luke, L. Y. He, and M. Zhang, *Optica* **8**, 357 (2021).
- C. Xiong, W. H. P. Pernice, and H. X. Tang, *Low-Loss, Silicon Integrated, Nano Lett* **12**, 3562 (2012).
- J. Mao, F. Uemura, S. A. Yazdani, Y. Yin, H. Sato, G.-W. Lu, and S. J. C. M. Yokoyama, *Commun. Mat* **5**, 114 (2024).
- L. Chen, Q. Xu, M. G. Wood, and R. M. Reano, *Hybrid silicon and lithium niobate electro-optical ring modulator*, *Optica* **1**, 112 (2014).
- C. Wang, M. Zhang, B. Stern, M. Lipson, and M. Loncar, *Opt. Express* **26**, 1547 (2018).

References

1. D. A. B. Miller, Attojoule Optoelectronics for Low-Energy Information Processing and Communications, *J. Lightwave Technol.* **35**, 346 (2017).
2. C. Sun, M. T. Wade, Y. Lee, J. S. Orcutt, L. Alloatti, M. S. Georgas, A. S. Waterman, J. M. Shainline, R. R. Avizienis, S. Lin, B. R. Moss, R. Kumar, F. Pavanello, A. H. Atabaki, H. M. Cook, A. J. Ou, J. C. Leu, Y. H. Chen, K. Asanovic, R. J. Ram, M. A. Popovic, and V. M. Stojanovic, Single-chip microprocessor that communicates directly using light, *Nature* **528**, 534 (2015).
3. X. D. Zheng, P. Y. Zhang, R. Y. Ge, L. L. Lu, G. L. He, Q. Chen, F. C. Qu, L. B. Zhang, X. L. Cai, Y. Q. Lu, S. N. Zhu, P. H. Wu, and X. S. Ma, Heterogeneously integrated, superconducting silicon-photonic platform for measurement-device-independent quantum key distribution, *Adv. Photonics* **3**, 10 (2021).
4. Y. H. Zhao, X. Wang, D. S. Gao, J. J. Dong, and X. L. Zhang, On-chip programmable pulse processor employing cascaded MZI-MRR structure, *Front. Optoelectron.* **12**, 148 (2019).
5. Q. F. Xu, B. Schmidt, S. Pradhan, and M. Lipson, Micrometre-scale silicon electro-optic modulator, *Nature* **435**, 325 (2005).
6. J. Liu, M. Beals, A. Pomerene, S. Bernardis, R. Sun, J. Cheng, L. C. Kimerling, and J. Michel, Waveguide-integrated, ultralow-energy GeSi electro-absorption modulators, *Nat. Photonics* **2**, 433 (2008).
7. M. B. He, M. Y. Xu, Y. X. Ren, J. Jian, Z. L. Ruan, Y. S. Xu, S. Q. Gao, S. H. Sun, X. Q. Wen, L. D. Zhou, L. Liu, C. J. Guo, H. Chen, S. Y. Yu, L. Liu, and X. L. Cai, High-performance hybrid silicon and lithium niobate Mach-Zehnder modulators for 100 Gbit s⁻¹ and beyond, *Nat. Photonics* **13**, 359 (2019).
8. L. P. Gu, B. B. Wang, Q. C. Yuan, L. Fang, Q. Zhao, X. T. Gan, and J. L. Zhao, Fano resonance from a one-dimensional topological photonic crystal, *APL Photonics* **6**, 6 (2021).
9. Y. He, Y. Zhang, Q. M. Zhu, S. H. An, R. Y. Cao, X. H. Guo, C. Y. Qiu, and Y. K. Su, Silicon High-Order Mode (De)Multiplexer on Single Polarization, *J. Lightwave Technol.* **36**, 5746 (2018).
10. G. T. Reed, G. Mashanovich, F. Y. Gardes, and D. J. Thomson, Silicon optical modulators, *Nat. Photonics* **4**, 518 (2010).
11. M. Zhang, C. Wang, P. Kharel, D. Zhu, and M. Loncar, Integrated lithium niobate electro-optic modulators: when performance meets scalability, *Optica* **8**, 652 (2021).
12. Y. Zhang, J. Shen, J. C. Li, H. W. Wang, C. L. Feng, L. Zhang, L. Sun, J. Xu, M. Liu, Y. Wang, Y. H. Tian, J. W. Dong, and Y. K. Su, High-speed electro-optic modulation in topological interface states of a one-dimensional lattice, *Light-Sci. Appl.* **12**, 10 (2023).
13. J. Shen, Y. Zhang, C. L. Feng, Z. H. Xu, L. Zhang, and Y. K. Su, Hybrid lithium tantalite-silicon integrated photonics platform for electro-optic modulation, *Opt. Lett.* **48**, 6176 (2023).
14. Z. H. Xu, Y. Zhang, J. Shen, Y. H. Dong, L. Y. Wu, J. Xu, and Y. K. Su, Hybrid aluminum nitride and silicon devices for integrated photonics, *Opt. Lett.* **47**, 4925 (2022).
15. S. Abel, F. Eltes, J. E. Ortmann, A. Messner, P. Castera, T. Wagner, D. Urbonas, A. Rosa, A. M. Gutierrez, D. Tulli, P. Ma, B. Bauerle, A. Josten, W. Heni, D. Caimi, L. Czornomaz, A. A. Demkov, J. Leuthold, P. Sanchis, and J. Fompeyrine, Large Pockels effect in micro-and nanostructured barium titanate integrated on silicon, *Nat. Mater.* **18**, 42 (2019).
16. G. Y. Chen, Y. Gao, H. L. Lin, and A. J. Danner, Compact and Efficient Thin-Film Lithium Niobate Modulators, *Adv. Photon. Res.* **4**, 15 (2023).
17. X. H. Du, J. H. Zheng, U. Belegundu, and K. Uchino, Crystal orientation dependence of piezoelectric properties of lead zirconate titanate near the morphotropic phase boundary, *Appl. Phys. Lett.* **72**, 2421 (1998).
18. D. S. Ban, G. L. Liu, H. Y. Yu, X. Y. Sun, N. P. Deng, and F. Qiu, High electro-optic coefficient lead zirconate titanate films toward low-power and compact modulators, *Opt. Mater. Express* **11**, 1733 (2021).
19. K. Alexander, J. P. George, J. Verbist, K. Neyts, B. Kuyken, D. Van Thourhout, and J. Beeckman, Nanophotonic Pockels modulators on a silicon nitride platform, *Nat. Commun.* **9**, 6 (2018).
20. G. L. Liu, H. Y. Yu, D. S. Ban, B. Li, G. Q. Wei, C. Yang, J. G. Wang, Y. I. Sohn, Y. Han, and F. Qiu, Highly efficient lead zirconate titanate ring modulator, *APL Photonics* **9**, 6 (2024).
21. P. Kharel, C. Reimer, K. Luke, L. Y. He, and M. Zhang, Breaking voltage-bandwidth limits in integrated lithium niobate modulators using micro-structured electrodes, *Optica* **8**, 357 (2021).
22. C. Xiong, W. H. P. Pernice, and H. X. Tang, Low-Loss, Silicon Integrated, Aluminum Nitride Photonic Circuits and Their Use for Electro-Optic Signal Processing, *Nano Lett.* **12**, 3562 (2012).
23. J. Mao, F. Uemura, S. A. Yazdani, Y. Yin, H. Sato, G.-W. Lu, and S. J. C. M. Yokoyama, Ultra-fast perovskite electro-optic modulator and multi-band transmission up to 300 Gbit s⁻¹, *Commun. Mat.* **5**, 114 (2024).
24. L. Chen, Q. Xu, M. G. Wood, and R. M. Reano, Hybrid silicon and lithium niobate electro-optical ring modulator, *Optica* **1**, 112 (2014).
25. C. Wang, M. Zhang, B. Stern, M. Lipson, and M. Loncar, Nanophotonic lithium niobate electro-optic modulators, *Opt. Express* **26**, 1547 (2018).